Crystallization kinetics and glass-forming ability of bulk metallic glasses $Pd_{40}Cu_{30}Ni_{10}P_{20}$ and $Zr_{41.2}Ti_{13.8}Cu_{12.5}Ni_{10}Be_{22.5}$ from classical theory

Donghua Xu[1,2,*] and William L. Johnson[1]
[1]*Division of Engineering and Applied Science, Mail Code 138-78, California Institute of Technology, Pasadena, California 91125, USA*
[2]*Department of Nuclear Engineering, University of California, Berkeley, California 94720-1730, USA*
(Received 19 March 2006; revised manuscript received 13 April 2006; published 27 July 2006)

Due to their scientific significance and potential engineering applications, bulk metallic glasses are among the most intensively studied advanced materials. Understanding the glass-forming ability (GFA) of these metallic alloys is a long-standing subject. While a large number of empirical factors have been proposed to correlate with GFA of the alloys, a full understanding of GFA remains a goal to achieve. Since glass formation is a competing process against crystallization, we have performed a systematic analysis on the crystallization kinetics of two known best metallic glass-formers $Pd_{40}Cu_{30}Ni_{10}P_{20}$ (in at. %) and $Zr_{41.2}Ti_{13.8}Cu_{12.5}Ni_{10}Be_{22.5}$ based on classical nucleation and growth theory. Our results show that there is a dramatic difference between the two alloys in their nucleation behavior although they possess comparable GFA. Particularly, an extremely sharp nucleation peak ($\sim 10^{18}/m^3$ s) is found for $Pd_{40}Cu_{30}Ni_{10}P_{20}$ around 632 K with a very small half maximum width of 42 K, implying that this alloy is an excellent candidate for nanocrystallization studies. Moreover, we have also found that the GFA of these alloys can be calculated to a high accuracy and precision based on the classical theory, suggesting that the classical theory may be sufficient to account for glass formation mechanism in these metallic alloys.

DOI: 10.1103/PhysRevB.74.024207 PACS number(s): 61.43.Dq, 81.05.Kf, 81.05.Bx, 81.30.Fb

I. INTRODUCTION

Because of their unique structure and properties, bulk metallic glasses (BMGs), a new category of advanced materials, are receiving tremendous attention from both fundamental and practical research disciplines. Glass-forming ability (GFA) is one of the most important subjects in the study of BMGs, because it determines, to a large degree, the potential for this new category of materials to be utilized in various applications.[1–8] Upon continuous cooling from its molten state, an alloy can eventually form a glass if, and only if, the cooling rate exceeds a critical value. This critical cooling rate (R_c) is a direct and universal measurement of the GFA of any substance including the conventional oxide glasses. Therefore, a complete understanding of GFA should ultimately be supported by an accurate and precise calculation of the R_c. While a large number of empirical factors (e.g., Refs. 9–14) have been proposed over the past decades to correlate with the GFA of various metallic glasses, they either were not verified against R_c or could not reproduce the experimentally measured R_c to a satisfactory accuracy and precision. The accurate and precise calculation of R_c, and accordingly, the full understanding of metallic glass formation mechanism remain unaccomplished.

Considering that glass formation is a competing process against crystallization, we perform a systematic study on the crystal nucleation and growth kinetics of two known best metallic glass formers $Pd_{40}Cu_{30}Ni_{10}P_{20}$ (in at. %) and $Zr_{41.2}Ti_{13.8}Cu_{12.5}Ni_{10}Be_{22.5}$ based on classical theory. We also calculate the R_c values for the two alloys by virtue of a continuous integral method (first introduced by Weinberg *et al.*[15] for oxide glasses) in the framework of the classical theory, and analyze the accuracy and precision of the R_c calculation.

II. CRYSTAL NUCLEATION AND GROWTH KINETICS

A. $Pd_{40}Cu_{30}Ni_{10}P_{20}$

$Pd_{40}Cu_{30}Ni_{10}P_{20}$ and $Zr_{41.2}Ti_{13.8}Cu_{12.5}Ni_{10}Be_{22.5}$ were selected for this study primarily because of the availability of their thermodynamic and kinetic data as well as reliable R_c values determined directly from continuous cooling experiments.[16–19]

In Ref. 16, the isothermal temperature-time-transformation (TTT) diagram of $Pd_{40}Cu_{30}Ni_{10}P_{20}$ was measured and successfully fitted to the classical nucleation and growth theory using the following equations:

$$I_v = \frac{A_v}{\eta} \exp\left(-\frac{16\pi\sigma^3}{3k_B T \Delta G^2}\right), \tag{1}$$

$$u = \frac{k_B T}{3\pi l^2 \eta}\left[1 - \exp\left(-\frac{n\Delta G}{k_B T}\right)\right], \tag{2}$$

and

$$t = \left(\frac{3f_c}{\pi I_v u^3}\right)^{1/4}, \tag{3}$$

where I_v is the steady-state nucleation rate, u is the diffusion-controlled crystal growth rate, A_v is a fitting parameter, η is the temperature-dependent viscosity, k_B is the Boltzmann constant, σ and ΔG are the interfacial energy per area and the Gibbs free energy difference per volume between the liquid and the crystalline phases, respectively, l is the average atomic diameter, n is the average atomic volume, and f_c is the critical crystallized volume fraction detectable by instruments (f_c is usually assigned to a somewhat arbitrary value for the fitting of a TTT diagram, and A_v and σ are the only two fitting parameters. The choice of f_c value, however, does not affect the fitting [Eq. (3)] or the calculation of R_c

TABLE I. Thermodynamic and kinetic data for $Pd_{40}Cu_{30}Ni_{10}P_{20}$ (taken from Ref. 16).

η_0 (Pa s)	D	T_0 (K)	ΔH_F (J/m^3)	T_l (K)	σ (J/m^2)	A_v (Pa/m^3)	n (m^3)	l (m)	f_c	T_g (K)	T_n (K)	t_n (s)
9.34×10^{-3}	9.25	447	7.69×10^{8}	823	0.061[a]	4.4×10^{31}	1.52×10^{-29}	3.1×10^{-10}	0.005	582	680	50

[a]The value of 0.067 J/m^2 for σ given in Ref. 16 is not accurate.

[Eq. (8) below] because the intrinsic fitting parameter besides σ is actually the ratio A_v/f_c rather than A_v. It does, on the other hand, affect the absolute value of I_ν [Eq. (1)] through A_v). In the fitting, a Vogel-Fulcher-Tamman (VFT) form was used to represent the temperature dependence of viscosity

$$\eta(T) = \eta_0 \exp\left(\frac{DT_0}{T - T_0}\right), \tag{4}$$

where η_0, D, and T_0 are three constants. In addition, a first order approximation was used for ΔG, i.e., $\Delta G = \Delta H_F(1 - T/T_l)$, where ΔH_F is the enthalpy of fusion per unit volume, and T_l is the liquidus temperature.

Table I summarizes all the relevant thermodynamic and kinetic data for $Pd_{40}Cu_{30}Ni_{10}P_{20}$ taken from Ref. 16. Using these data, one can calculate and plot the nucleation rate I_ν and the growth rate u as functions of temperature. The results are shown in Fig. 1. Upon cooling from the liquidus temperature 823 K, the crystal growth rate increases immediately and quickly reaches its maximum value of 3.2×10^{-7} m/s at 794 K, and then drops rapidly afterwards. By contrast, the nucleation rate remains very low over a relatively large temperature interval of ~123 K below the liquidus temperature. Starting from ~700 K, however, the nucleation rate rises steeply as the temperature further decreases, and rapidly assumes its maximum value of 10^{18}/m^3 s at 632 K, followed by a steep decrease afterwards.

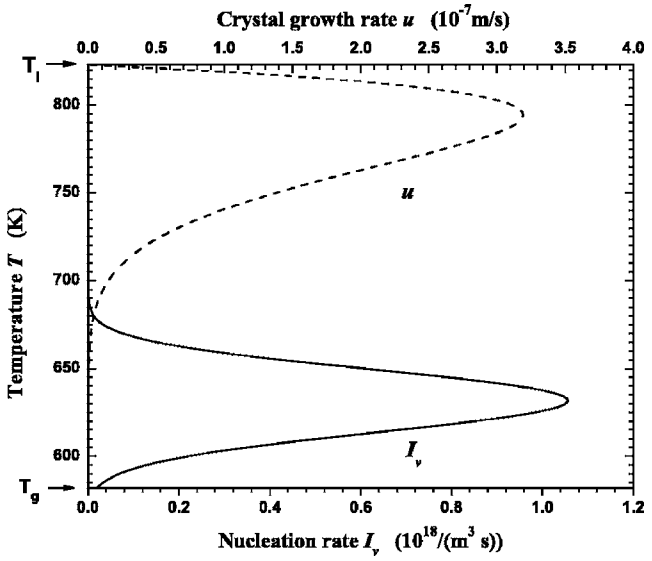

FIG. 1. Nucleation rate I_ν and crystal growth rate u as functions of temperature for $Pd_{40}Cu_{30}Ni_{10}P_{20}$.

Both the nucleation rate and the growth rate are jointly controlled by thermodynamics and kinetics. In fact, one can separate the thermodynamic and kinetic factors by dividing each of the rates into two parts, with η representing kinetics and $I_\nu\eta$ (or $u\eta$) representing thermodynamics. Figure 2 shows the plots of the two thermodynamic factors, for the nucleation rate and the growth rate of $Pd_{40}Cu_{30}Ni_{10}P_{20}$, respectively. It can be seen that within the temperature range between the liquidus temperature and the glass transition temperature (T_g, 582 K for $Pd_{40}Cu_{30}Ni_{10}P_{20}$, refer to Table I), the two thermodynamic factors both increase monotonically as temperature decreases, which means that thermodynamics consistently enhances crystal nucleation and growth. On the other hand, kinetics consistently restrains crystal nucleation and growth, as represented by monotonically increasing η (plot not shown) during continuous cooling process. It is the competition between thermodynamics and kinetics that has resulted in the peaks of I_ν and u that are shown in Fig. 1.

As we will discuss in next section, when compared with $Zr_{41.2}Ti_{13.8}Cu_{12.5}Ni_{10}Be_{22.5}$, the nucleation behavior of $Pd_{40}Cu_{30}Ni_{10}P_{20}$ appears very unique and has important implications for future nanocrystallization studies.

B. $Zr_{41.2}Ti_{13.8}Cu_{12.5}Ni_{10}Be_{22.5}$

In Ref. 17, the kinetic time scales for viscous flow, atomic transport, and crystallization (isothermal) in the liquid and

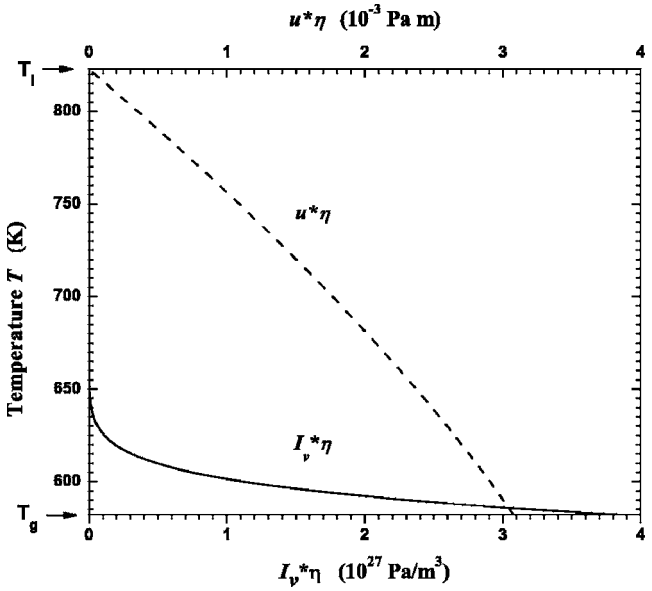

FIG. 2. Thermodynamic factors, $I_\nu\eta$ and $u\eta$, for the nucleation rate I_ν and the crystal growth rate u, respectively, as functions of temperature for $Pd_{40}Cu_{30}Ni_{10}P_{20}$.

TABLE II. Thermodynamic and kinetic data for $Zr_{41.2}Ti_{13.8}Cu_{12.5}Ni_{10}Be_{22.5}$ (taken from Ref. 17 unless otherwise noted).

η_0 (Pa s)	c_1 (K)	c_2 (K)	T_0 (K)	D_0 (m^2/s)	Q_{eff} (eV)	ΔH_F (J/m^3)	T_l (K)	σ (J/m^2)	A_v (m^{-5})	n (m^3)	l (m)	f_c	T_g (K)	T_n (K)	t_n (s)
4×10^{-5}	9866	162	672	6.85×10^{-8}	1.2	7.9×10^{8}[a]	1026	0.04	3×10^{20}	1.72×10^{-29}	3.2×10^{-10}	10^{-4}	620[a]	895	60

[a]Taken from Ref. 19.

supercooled liquid states of $Zr_{41.2}Ti_{13.8}Cu_{12.5}Ni_{10}Be_{22.5}$ (Vitreloy-1) were reported. It was found that the measured viscosity of Vitreloy-1 cannot be fitted well by a VFT equation in the supercooled liquid range. Rather, the Cohen-Grest (CG) free volume model[20] provides a better description for the temperature dependence of viscosity, i.e.

$$\eta = \eta_0 \exp(c_1/[T - T_0 + \sqrt{(T-T_0)^2 + c_2 T}]). \quad (5)$$

The measured isothermal TTT diagram was fitted well using Eq. (3) and the following expressions for the nucleation rate I_ν and the crystal growth rate u:

$$I_\nu = A_v D_{eff} \exp\left(-\frac{16\pi\sigma^3}{3k_B T \Delta G^2}\right) \quad (6)$$

and

$$u = \frac{D_{eff}}{l}\left[1 - \exp\left(-\frac{n\Delta G}{k_B T}\right)\right], \quad (7)$$

where D_{eff} is a piecewise-defined effective diffusivity: above 850 K, the effective diffusivity obeys a Stokes-Einstein relationship with viscosity, i.e., $D_{eff}=k_BT/(3\pi l\eta)$; below 850 K, however, the effective diffusivity is better described by an Arrhenius law, i.e., $D_{eff}=D_0\exp(-Q_{eff}/k_BT)$ with an activation energy $Q_{eff}=1.2$ eV.

Table II provides a list of the relevant data for Vitreloy-1 taken from Refs. 17 and 19. The nucleation rate I_ν and the crystal growth rate u are plotted versus temperature in Fig. 3. The general profiles of I_ν and u for Vitreloy-1 are very similar to those for $Pd_{40}Cu_{30}Ni_{10}P_{20}$, both increasing initially as temperature decreases, reaching a peak value and then decreasing subsequently. The peak positions of I_ν and u for Vitreloy-1 are 793 K and 989 K, respectively.

More careful comparison of Vitreloy-1 with $Pd_{40}Cu_{30}Ni_{10}P_{20}$, however, reveals that while the maximum crystal growth rates for the two alloys are different by only two orders of magnitude, the maximum nucleation rates differ by almost fourteen orders of magnitude (Note that there is a factor of 50 difference between the f_c values used for the two alloys, which may affect I_ν by the same factor through A_v. However, this cannot at all account for the ~14 orders of magnitude difference in the two maximum nucleation rates.). Nevertheless, the two alloys show very similar shortest crystallization time, i.e., "nose time" t_n, on their measured isothermal TTT diagrams, being 50 s and 60 s for $Pd_{40}Cu_{30}Ni_{10}P_{20}$ and for Vitreloy-1, respectively.[16,17] This has resulted from the different degree of overlapping and the different sharpness (with respect to temperature) of I_ν and u for the two alloys. Particularly worth noting is the distinct sharpness of the I_ν peak for $Pd_{40}Cu_{30}Ni_{10}P_{20}$, being characterized by its very small half maximum width of 42 K and extremely high magnitude of $\sim10^{18}/m^3$ s, as compared to 131 K and $2.3\times10^4/m^3$ s, respectively, for Vitreloy-1 (refer to Fig. 1, Fig. 3, and also Table III). From these results, one can expect that nanocrystallization can be obtained more easily in $Pd_{40}Cu_{30}Ni_{10}P_{20}$ than in Vitreloy-1. An extremely large number of nuclei will form when $Pd_{40}Cu_{30}Ni_{10}P_{20}$ is maintained at around 632 K, and yet they cannot easily grow into large grains due to the very low growth rate corresponding to that temperature. The characteristic data listed in Table III together with the information contained in Figs. 1–3 will provide important guidelines for future nanocrystallization experiments.

III. CALCULATION OF CRITICAL COOLING RATE

A. Continuous integral method

In Ref. 15, Weinberg *et al.* first utilized a continuous integral method to evaluate the relative effects of different factors (such as liquid-crystal interfacial energy σ) on the calculated critical cooling rate R_c for certain oxide glasses, on the basis of the Johnson-Mehl-Avrami (JMA) phase transformation model[21,22] and the classical theory for crystal nucleation and growth. In the method, assuming a spherical mode of crystal growth, the crystallized volume fraction f of a glass-forming liquid upon continuous cooling, if $f \ll 1$, depends on the cooling rate R as follows:

$$f = \frac{4\pi}{3R^4}\int_{T_l}^{T_g} I_\nu(T')dT'\left[\int_{T'}^{T_g} u(T'')dT''\right]^3.$$

Therefore, the critical cooling rate required for glass formation is determined as

TABLE III. Characteristics of the nucleation and growth peaks for $Pd_{40}Cu_{30}Ni_{10}P_{20}$ and $Zr_{41.2}Ti_{13.8}Cu_{12.5}Ni_{10}Be_{22.5}$. Notation: T_p—peak temperature, *HMW*—half maximum width.

Alloy Composition (at. %)	u_{max} (m/s)	T_p^u (K)	HMW^u (K)	$I_{v,max}$ ($m^{-3}\,s^{-1}$)	$T_p^{I_v}$ (K)	HMW^{I_v} (K)
$Pd_{40}Cu_{30}Ni_{10}P_{20}$	3.2×10^{-7}	794	60	1.1×10^{18}	632	42
$Zr_{41.2}Ti_{13.8}Cu_{12.5}Ni_{10}Be_{22.5}$	8.3×10^{-5}	989	80	2.3×10^{4}	793	131

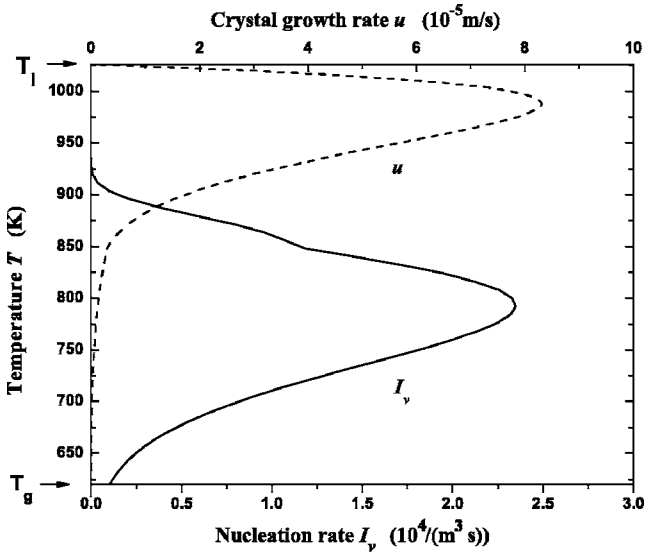

FIG. 3. Nucleation rate I_v and crystal growth rate u as functions of temperature for $Zr_{41.2}Ti_{13.8}Cu_{12.5}Ni_{10}Be_{22.5}$.

$$R_c = \left\{ \frac{4\pi}{3 f_c} \int_{T_l}^{T_g} I_v(T') dT' \left[\int_{T'}^{T_g} u(T'') dT'' \right]^3 \right\}^{1/4}. \quad (8)$$

By substituting Eqs. (1), (2), and (4) into Eq. (8) and using the data listed in Table I, the critical cooling rate R_c for $Pd_{40}Cu_{30}Ni_{10}P_{20}$ is calculated to be 0.46 K/s. This calculated value agrees remarkably well with the experimentally measured 0.33 K/s,[16] particularly considering the large variation, usually by several orders of magnitude, in the critical cooling rates of different metallic alloys.

Similarly, the critical cooling rate for Vitreloy-1 can be calculated using Eqs. (5)–(8), the piecewise-defined effective diffusivity D_{eff}, and the thermodynamic and kinetic data listed in Table II. The calculation yields R_c=0.91 K/s. As for the case of $Pd_{40}Cu_{30}Ni_{10}P_{20}$, this calculated value for Vitreloy-1 agrees strikingly well with the experimentally measured 1.4 K/s.[18]

B. Accuracy and precision of the calculations

It was warned in the original paper by Weinberg *et al.*[15] that small error in the interfacial energy σ may cause large uncertainty in the calculated R_c. For example, the authors demonstrated (see Fig. 3 in Ref. 15) when σ [proportional to a Turnbull's constant $\alpha=(N_A V_m^2)^{1/3}\sigma/\Delta H_F$ (Ref. 9)] increases by ~15%, the calculated R_c for SiO_2 drops by one order of magnitude. As a matter of fact, the use of the absolute value of the calculated R_c was not recommended by the authors.

However, the error (or, "sensitivity") analysis in Ref. 15 was performed in a way that errors from different factors were isolated and were not allowed to interfere with each other. Nevertheless, this is not the case when a measured isothermal TTT diagram (or part of it, particularly the part around its "nose") is available, as in the present study. In the present calculation of R_c, the measured TTT diagrams place constraints on the errors in σ and A_v. Take $Pd_{40}Cu_{30}Ni_{10}P_{20}$ as an example. As an illustration, Fig. 4 displays the experimental data together with three calculated TTT diagrams for $Pd_{40}Cu_{30}Ni_{10}P_{20}$. In Fig. 4, curve (b) is the best fit, with $A_v=4.4\times10^{31}$ Pa/m^3 and σ=0.061 J/m^2, curve (c) is calculated by fixing $A_v=4.4\times10^{31}$ Pa/m^3 and introducing 10% error to σ (and thus making σ=0.0671 J/m^2), and curve (d) is calculated using $A_v=5\times10^{34}$ Pa/m^3 and σ=0.0671 J/m^2 such that the nose time t_n is restored to the measured 50 s while keeping the 10% error in σ. Apparently, when introduced isolatedly, the 10% error can change the position of the calculated TTT diagram dramatically. In order to keep reasonable fit to the measured data, accordingly, the 10% error in σ has to be accommodated with a three orders of magnitude change in A_v. The mutually constrained errors in σ and A_v result in a fairly stabilized (precise) R_c, e.g., R_c=0.42 K/s for $A_v=5\times10^{34}$ Pa/m^3 and σ=0.0671 J/m^2, in comparison with R_c=0.46 K/s obtained using the best fit of σ and A_v.

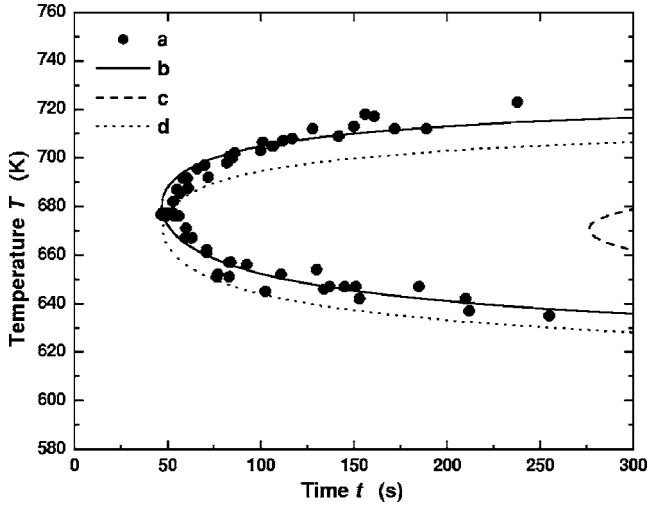

FIG. 4. Measured and calculated isothermal TTT diagrams of $Pd_{40}Cu_{30}Ni_{10}P_{20}$: (a) experimental data (Ref. 16); (b) calculated using $A_v=4.4\times10^{31}$ Pa/m^3 and σ=0.061 J/m^2; (c) calculated using $A_v=4.4\times10^{31}$ Pa/m^3 and σ=0.0671 J/m^2; (d) calculated using $A_v=5\times10^{34}$ Pa/m^3 and σ=0.0671 J/m^2.

A further extension to the above analysis is to allow ~±10 s uncertainties in the nose time t_n while keeping the 10% error in σ (i.e., fixing σ=0.0671 J/m^2). The calculated TTT diagrams are shown in Fig. 5. Correspondingly, the critical cooling rate is evaluated to be: R_c=0.34 K/s for $A_v=2\times10^{34}$ Pa/m^3, and R_c=0.60 K/s for $A_v=2\times10^{35}$ Pa/m^3.

Similar analysis has also been performed on Vitreloy-1. It is concluded that the error bars to the calculated R_c=0.46 K/s for $Pd_{40}Cu_{30}Ni_{10}P_{20}$ and R_c=0.91 K/s for Vitreloy-1, caused by the uncertainties in their measured TTT diagrams, are both within ±0.2 K/s. Therefore, the calculation is very precise. On the other hand, comparing the calculated values with the measured 0.33 K/s and 1.4 K/s for $Pd_{40}Cu_{30}Ni_{10}P_{20}$ and Vitreloy-1, respectively, indicates the high accuracy of the calculation.

Certain empirical methods, such as the Turnbull's T_{rg} rule[9] and the one based on the γ parameter,[10] have been used frequently to obtain a quick and rough estimation of GFA since they do not require all the data input as needed for the

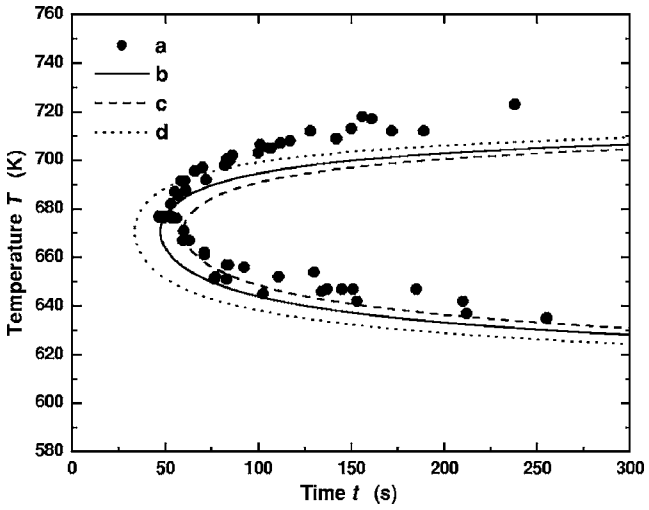

FIG. 5. Measured and calculated (with fixed $\sigma=0.0671$ J/m^2) isothermal TTT diagrams of $Pd_{40}Cu_{30}Ni_{10}P_{20}$: (a) experimental data (Ref. 16); (b) calculated using $A_v=5\times10^{34}$ Pa/m^3; (c) calculated using $A_v=2\times10^{34}$ Pa/m^3; (d) calculated using $A_v=2\times10^{35}$ Pa/m^3.

integral method and accordingly much simpler to apply. While many alloy systems were reported to support the "predictive power" of the empirical methods, there were also a comparable number of exceptions with distinct deviations. It should be noted that the main concern here in this present paper is to obtain a more complete and accurate fundamental understanding of why a metallic glass can form from thermodynamic and kinetic point of view, rather than to establish another quick and rough criterion that will almost certainly encounter many exceptions.

IV. CONCLUSIONS

Within the framework of classical nucleation and growth theory, we have performed a systematic study on the crystallization kinetics of two known best metallic glass formers $Pd_{40}Cu_{30}Ni_{10}P_{20}$ and $Zr_{41.2}Ti_{13.8}Cu_{12.5}Ni_{10}Be_{22.5}$, and calculated the critical cooling rates (R_c) for the two alloys using a continuous integral method. We have found the existence of an extremely sharp nucleation peak ($\sim10^{18}$/m^3 s) around 632 K for $Pd_{40}Cu_{30}Ni_{10}P_{20}$ with a very small half maximum width of 42 K, which implies that this alloy is an excellent candidate for nanocrystallization studies. The calculated R_c values agree remarkably well with experimental measurements, with only very small deviation of 0.13 K/s and 0.5 K/s for $Pd_{40}Cu_{30}Ni_{10}P_{20}$ and $Zr_{41.2}Ti_{13.8}Cu_{12.5}Ni_{10}Be_{22.5}$, respectively. The error bars for the calculations, caused by the uncertainties in the measured TTT diagrams, are evaluated to be within ±0.2 K/s for both alloys. The high accuracy and precision of the calculations suggest that the classical theory may be sufficient to account for glass formation mechanism in these metallic alloys.

ACKNOWLEDGMENTS

D. H. Xu would like to thank B. D. Wirth at the University of California at Berkeley for his financial support and valuable discussions. J. F. Loffler at ETH (Zurich) and J. Schroers at Yale University are acknowledged for providing some of the original data. E. Ma at Johns Hopkins University is appreciated for proofreading the manuscript.

*Corresponding author. Email address: xudh@berkeley.edu

[1] W. L. Johnson, MRS Bull. **24**, 42 (1999).
[2] D. Xu, G. Duan, and W. L. Johnson, Phys. Rev. Lett. **92**, 245504 (2004).
[3] Y. He, S. J. Poon, and G. J. Shiflet, Science **241**, 1640 (1988).
[4] V. Ponnambalam, S. J. Poon, and G. J. Shiflet, J. Mater. Res. **19**, 1320 (2004).
[5] B. Zhang, R. J. Wang, D. Q. Zhao, M. X. Pan, and W. H. Wang, Phys. Rev. B **70**, 224208 (2004).
[6] J. Das, M. B. Tang, K. B. Kim, R. Theissmann, F. Baier, W. H. Wang, and J. Eckert, Phys. Rev. Lett. **94**, 205501 (2005).
[7] H. W. Sheng, W. K. Luo, F. M. Alamgir, J. M. Bai, and E. Ma, Nature (London) **439**, 419 (2006).
[8] D. Xu, B. Lohwongwatana, G. Duan, W. L. Johnson, and C. Garland, Acta Mater. **52**, 2621 (2004).
[9] D. Turnbull, Contemp. Phys. **10**, 473 (1969).
[10] Z. P. Lu and C. T. Liu, Acta Mater. **50**, 3501 (2002).
[11] A. Inoue and A. Takeuchi, Mater. Trans., JIM **43**, 1892 (2002).
[12] D. N. Perera, J. Phys.: Condens. Matter **11**, 3807 (1999).
[13] Y. M. Wang *et al.*, Scr. Mater. **50**, 829 (2004).
[14] D. B. Miracle, W. S. Sanders, and O. N. Senkov, Philos. Mag. **83**, 2409 (2003).
[15] M. C. Weinberg, B. J. Zelinski, and D. R. Uhlmann, J. Non-Cryst. Solids **123**, 90 (1990).
[16] J. F. Loffler, J. Schroers, and W. L. Johnson, Appl. Phys. Lett. **77**, 681 (2000).
[17] A. Masuhr, T. A. Waniuk, R. Busch, and W. L. Johnson, Phys. Rev. Lett. **82**, 2290 (1999).
[18] T. A. Waniuk, J. Schroers, and W. L. Johnson, Appl. Phys. Lett. **78**, 1213 (2001).
[19] R. Busch, Y. J. Kim, and W. L. Johnson, J. Appl. Phys. **77**, 4039 (1995).
[20] G. S. Grest and M. H. Cohen, in *Advances in Chemical Physics*, edited by I. Prigogine and S. A. Rice (Wiley, New York, 1981), p. 455.
[21] W. A. Johnson and R. F. Mehl, Trans. AIME **135**, 416 (1939).
[22] M. Avrami, J. Chem. Phys. **7**, 1103 (1939).